Supporting Information for

Semiconductor-cluster-loaded ionic covalent organic nanosheets with enhanced photocatalytic reduction reactivity of nitroarenes

Jing-Ni Zhang,[a,†] Jia-Xing Liu, [a,†] Hao Ma,[a] Xiao Luo,[a] Cheng-Kun Han,[a] Rui Zhou,[b] Shang-Fu Yuan,[a,*] Dong-Sheng Li,[c] and Tao Wu[a,*]

[a]College of Chemistry and Materials Science, and Guangdong Provincial Key Laboratory of Functional Supramolecular Coordination Materials and Applications, Jinan University, Guangzhou, 510632, P. R. China

[b]Department of Developmental and Regenerative Biology, Jinan University, Guangzhou, 510632, P. R. China

[c]College of Materials and Chemical Engineering, Hubei Provincial Collaborative Innovation Center for New Energy Microgrid, Key Laboratory of Inorganic Nonmetallic Crystalline and Energy Conversion Materials, China Three Gorges University, Yichang, 443002, P. R. China

*Corresponding authors: sfyuan@jnu.edu.cn; wutao@jnu.edu.cn.

†These authors contributed equally.

I. Supporting figures

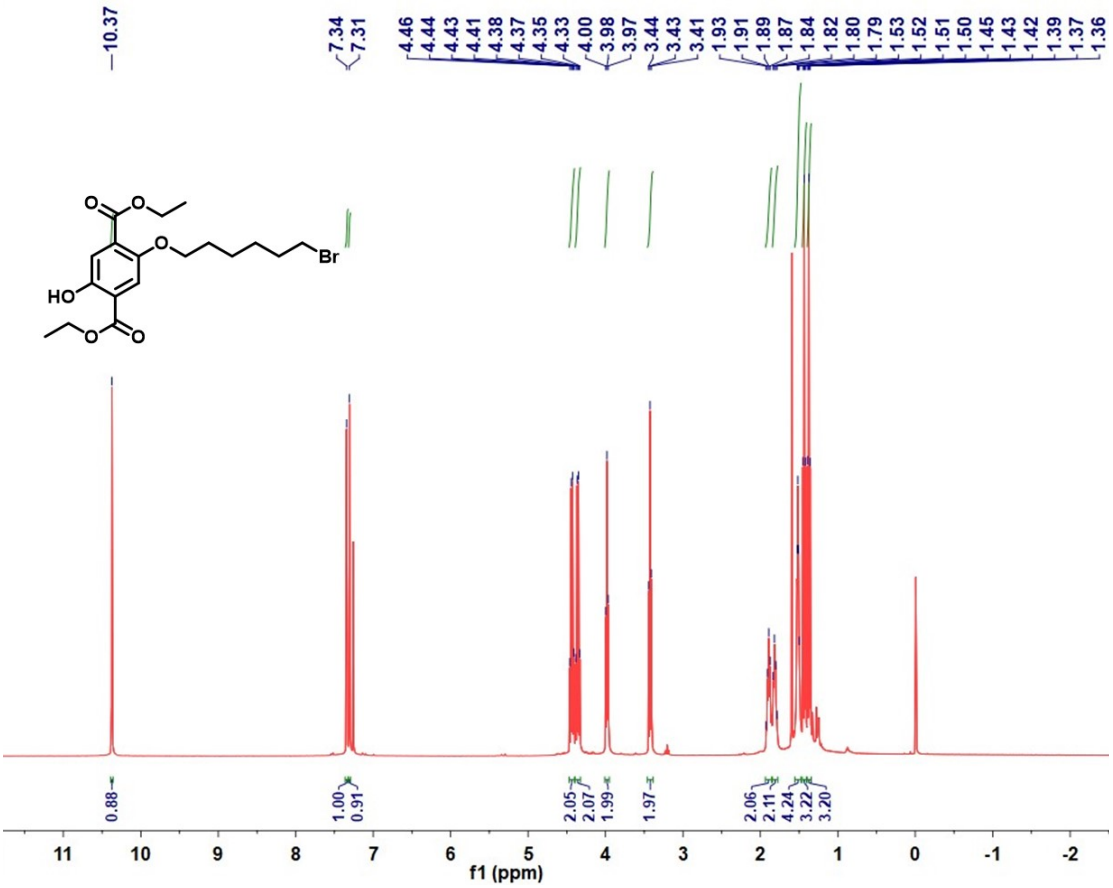

Figure S1. ^{1}H NMR of 2-hydroxy-5-(6-bromohexyloxy)-terephthalic acid diethyl ester (**1A**).

^{1}H NMR (400 MHz, $CDCl_3$) δ 10.37 (s, 1H), 7.34 (s, 1H), 7.31 (s, 1H), 4.43 (q, J = 7.1 Hz, 2H), 4.36 (q, J = 7.1 Hz, 2H), 3.98 (t, J = 6.3 Hz, 2H), 3.43 (t, J = 6.8 Hz, 2H), 1.90 (dd, J = 13.9, 6.9 Hz, 2H), 1.81 (dd, J = 13.3, 6.6 Hz, 2H), 1.51 (dd, J = 7.1, 3.4 Hz, 4H), 1.43 (t, J = 7.1 Hz, 3H), 1.37 (t, J = 7.1 Hz, 3H).

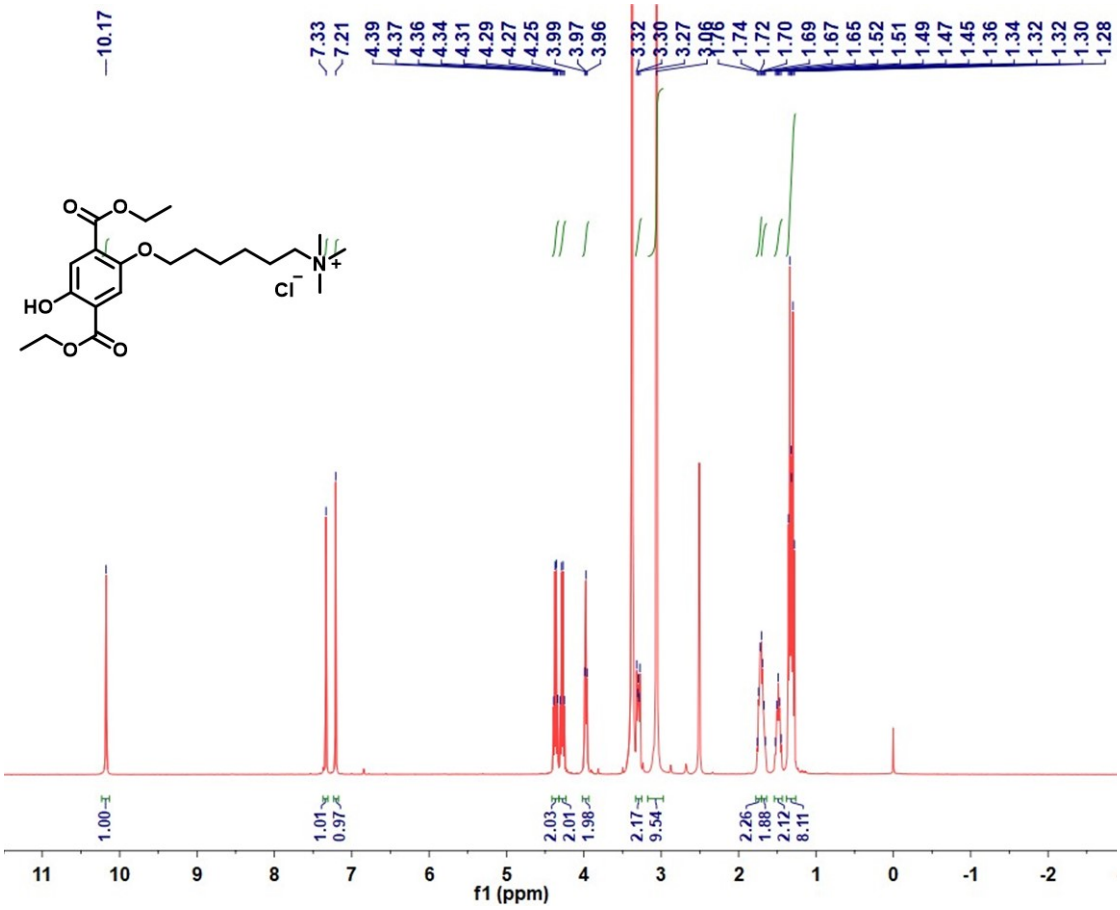

Figure S2. ^{1}H NMR of 2-hydroxy-5-(trimethylammonio-hexyloxy)-terephthalic acid diethyl ester (**2A**).

^{1}H NMR (400 MHz, DMSO) δ 10.17 (s, 1H), 7.33 (s, 1H), 7.21 (s, 1H), 4.36 (q, J = 7.1 Hz, 2H), 4.28 (q, J = 7.1 Hz, 2H), 3.97 (t, J = 6.1 Hz, 2H), 3.33 – 3.25 (m, 2H), 3.06 (s, 10H), 1.78 – 1.71 (m, 2H), 1.68 (dd, J = 14.1, 6.8 Hz, 2H), 1.49 (dt, J = 14.9, 7.4 Hz, 2H), 1.32 (dt, J = 16.4, 7.1 Hz, 8H).

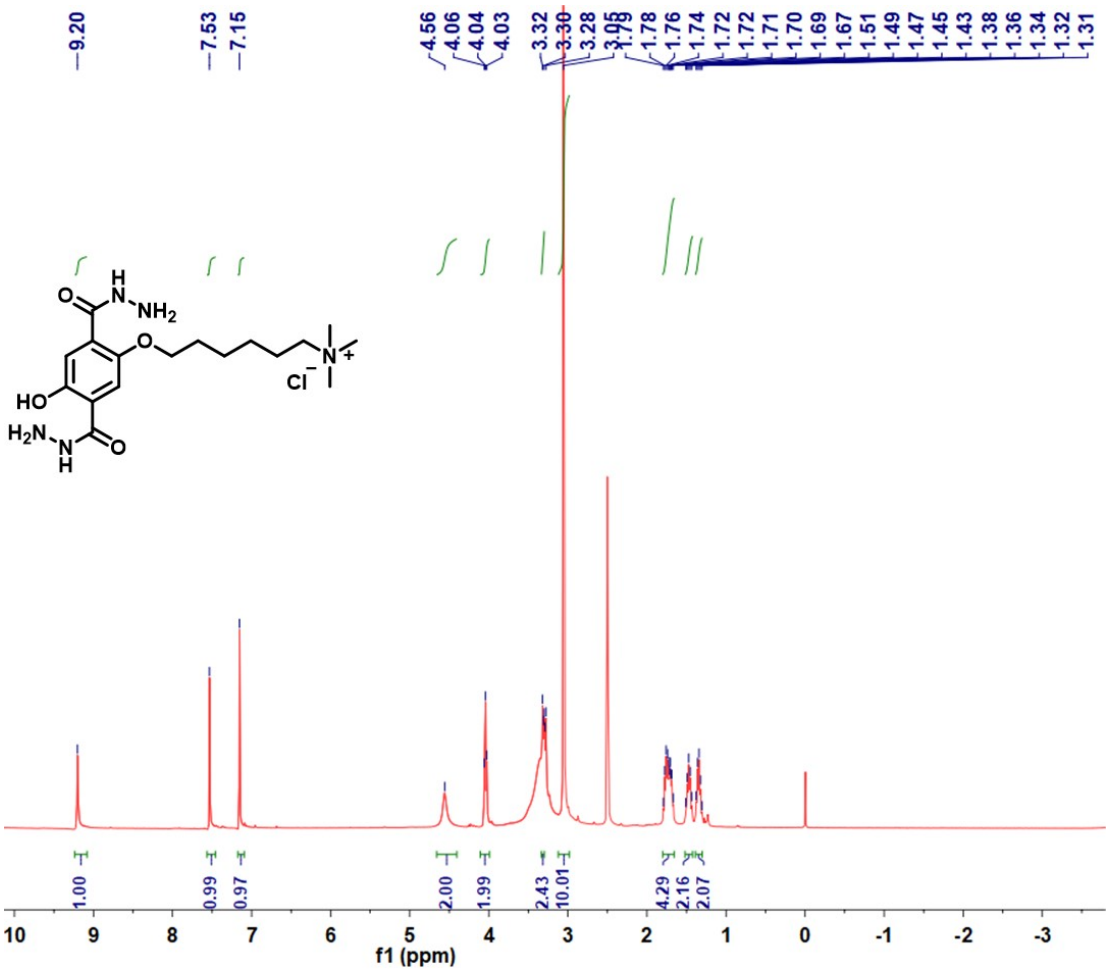

Figure S3. ^{1}H NMR of 2-hydroxy-5-(trimethylammonio-hexyloxy)-terephthalohydrazide (**3A**).

^{1}H NMR (400 MHz, DMSO) δ 9.20 (s, 1H), 7.53 (s, 1H), 7.15 (s, 1H), 4.56 (s, 2H), 4.04 (t, J = 6.3 Hz, 2H), 3.33 – 3.30 (m, 2H), 3.05 (s, 10H), 1.73 (dp, 4H), 1.47 (dt, J = 14.9, 7.3 Hz, 2H), 1.34 (dt, J = 14.4, 7.3 Hz, 2H).

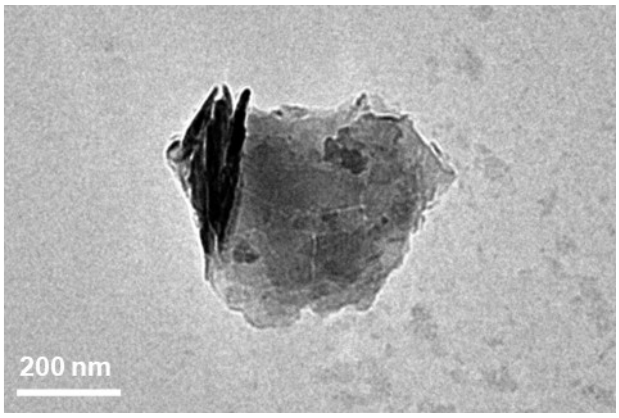

Figure S4. TEM images of **QA-CONs**.

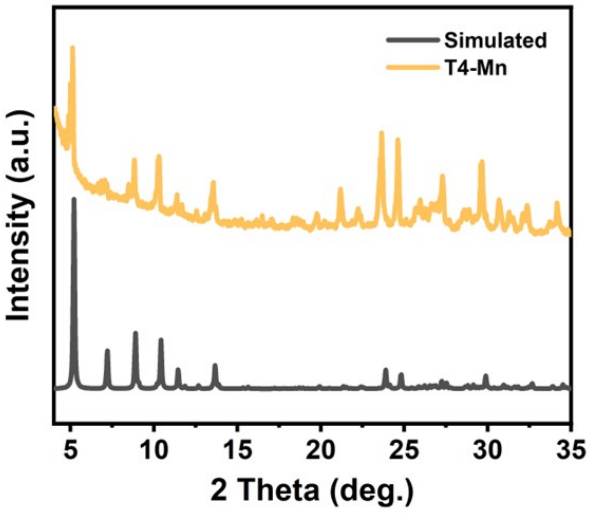

Figure S5. Experimental and simulated PXRD patterns of the **T4-Mn** crystals.

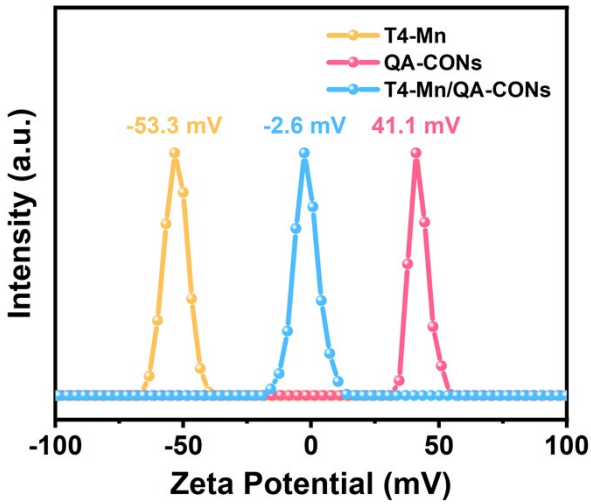

Figure S6. Zeta potentials for **T4-Mn**, **QA-CONs**, and **T4-Mn/QA-CONs**.

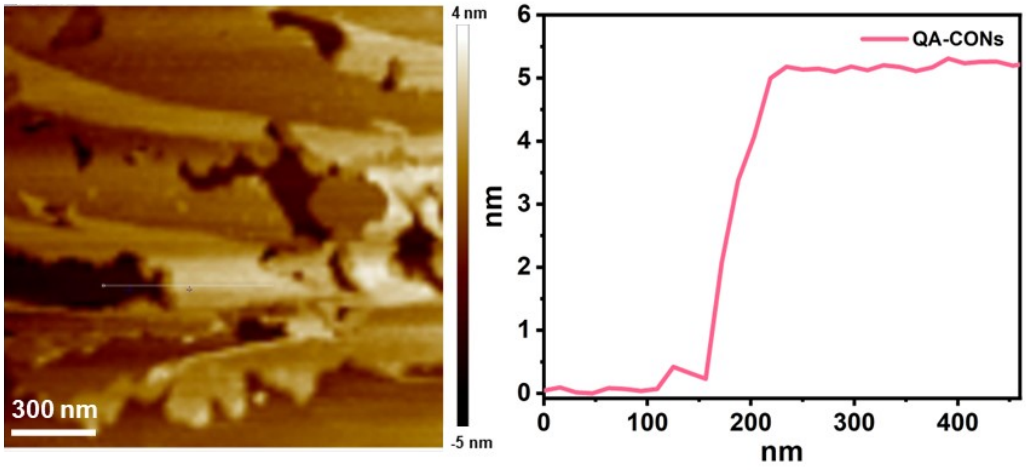

Figure S7. AFM image with the corresponding height profile of **QA-CONs**.

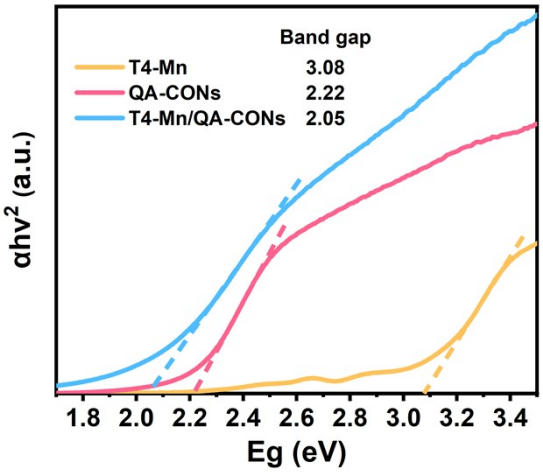

Figure S8. The Tauc plots of **T4-Mn**, **QA-CONs**, and the **T4-Mn/QA-CONs**.

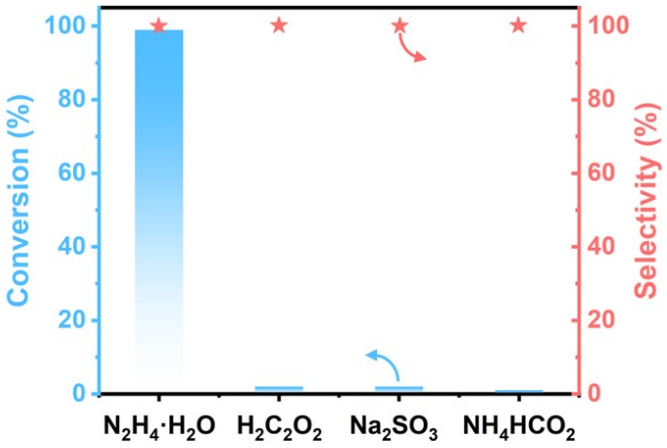

Figure S9. The effect of different sacrificial reagents of **T4-Mn/QA-CONs** on the nitrobenzene reduction performance.

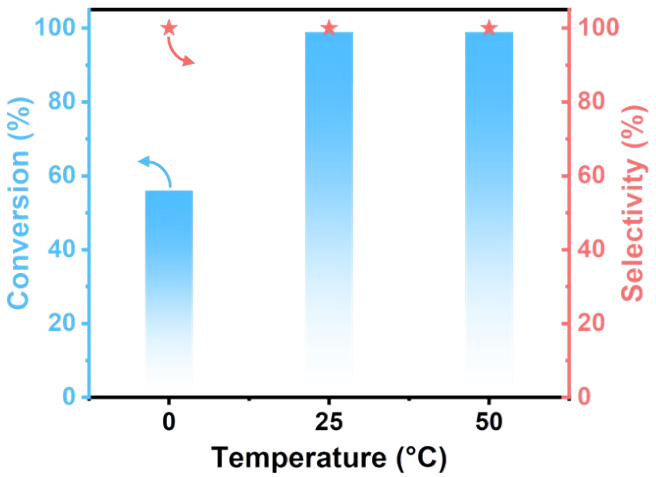

Figure S10. The effect of reaction temperature of **T4-Mn/QA-CONs** on the nitrobenzene reduction performance.

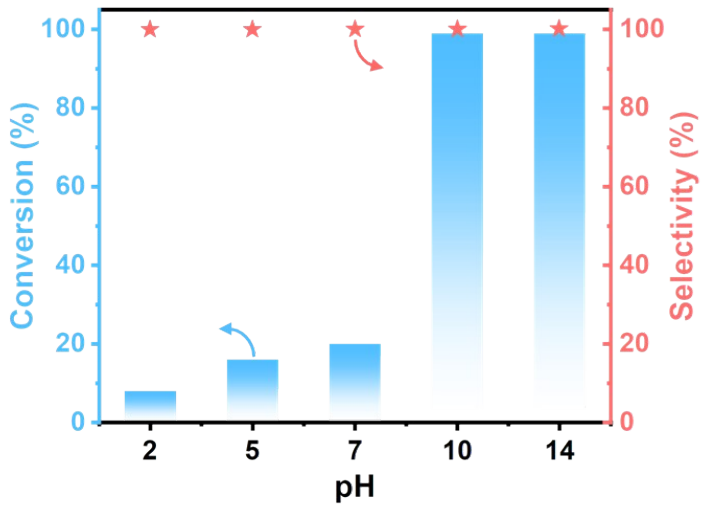

Figure S11. The effect of solution pH of **T4-Mn/QA-CONs** on the nitrobenzene reduction performance.

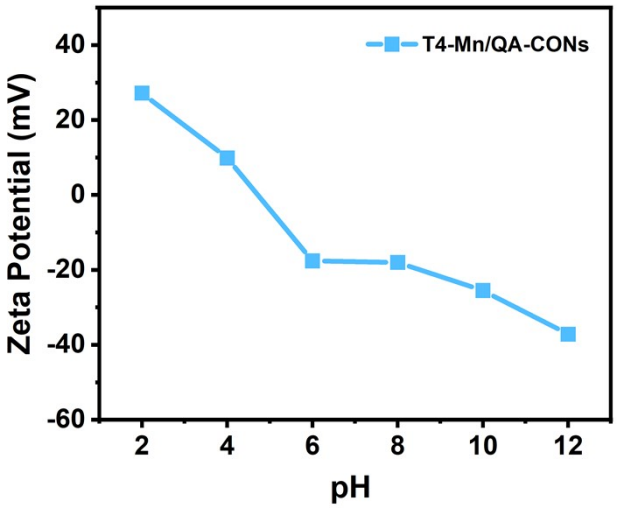

Figure S12. Zeta potential of **T4-Mn/QA-CONs** at various pH levels.

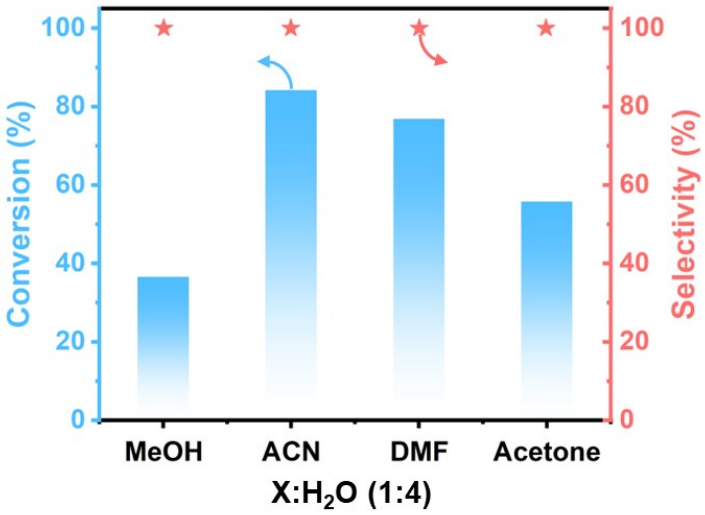

Figure S13. The photocatalytic nitrobenzene reduction performance of **T4-Mn/QA-CONs** in the different solvent systems under blue LEDs irradiation for 8 h.

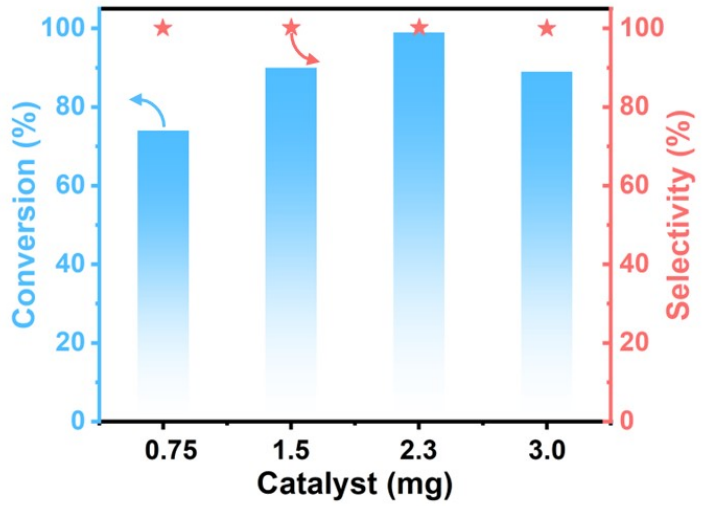

Figure S14. The effect of different concentrations of **T4-Mn/QA-CONs** on the nitrobenzene reduction performance.

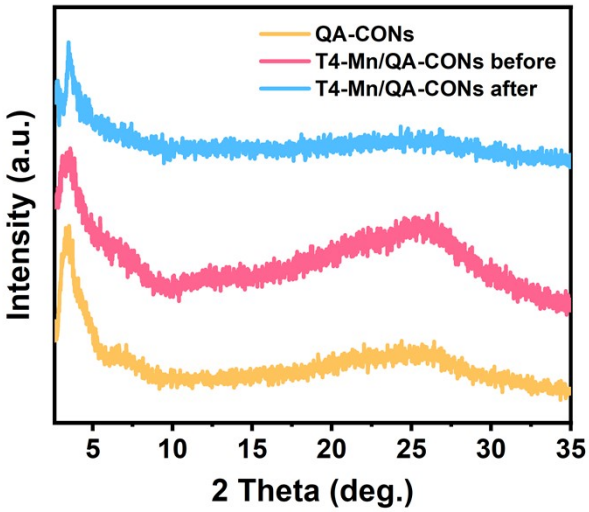

Figure S15. The experimental PXRD patterns of the **T4-Mn/QA-CONs** after the cycling tests.

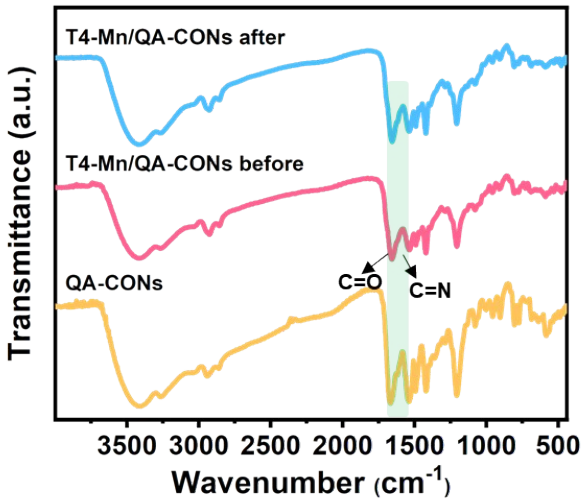

Figure S16. FTIR spectra of the **T4-Mn/QA-CONs** after the cycling tests.

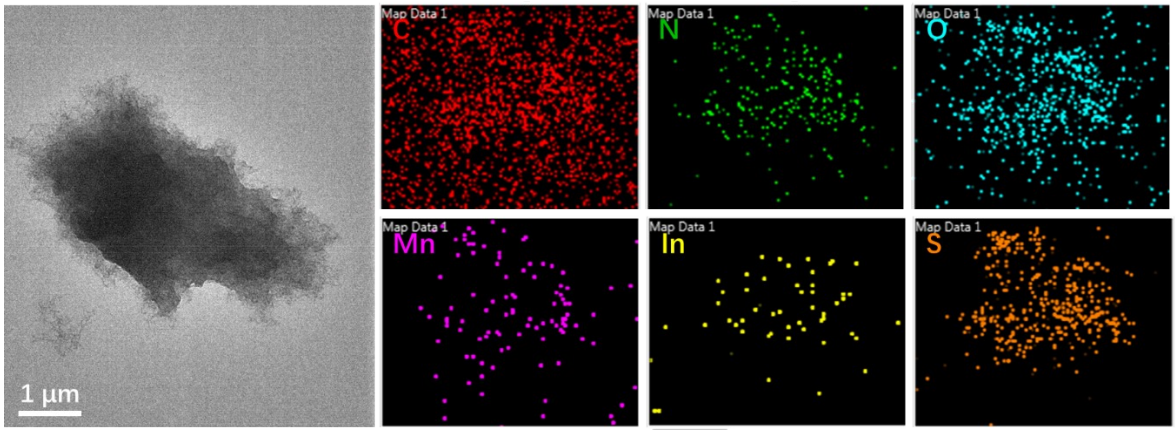

Figure S17. TEM element mapping images of the **T4-Mn/QA-CONs** after the photocatalytic reaction.

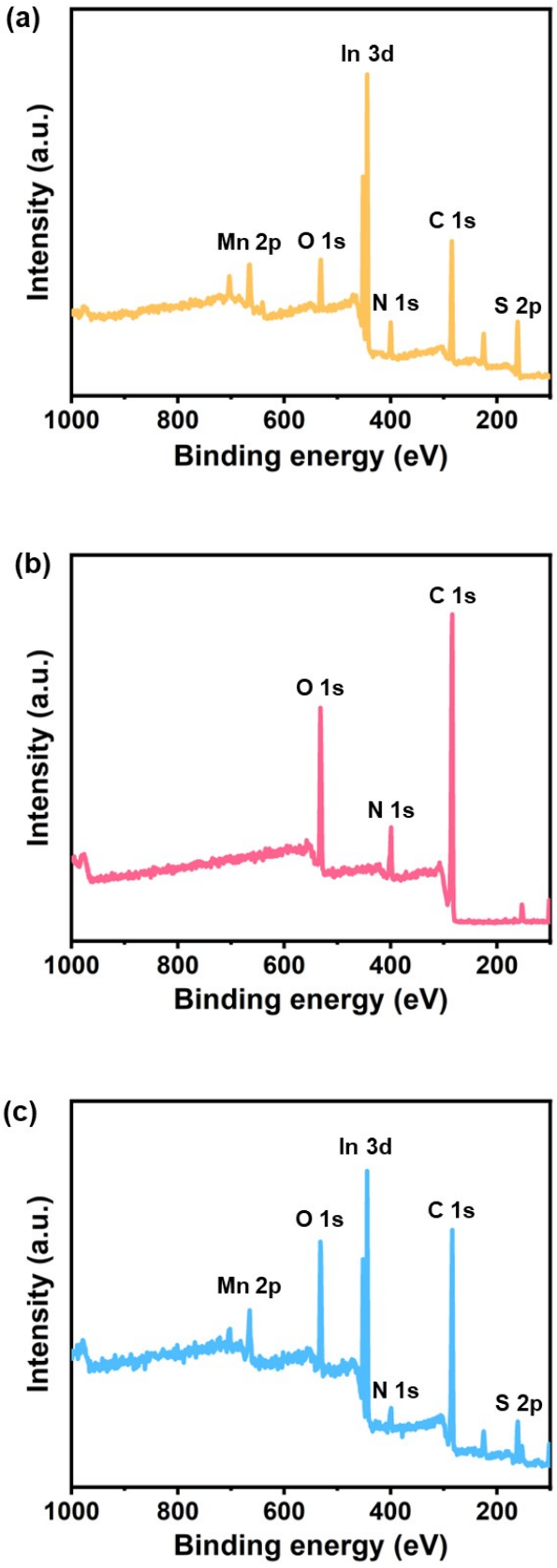

Figure S18. Full XPS spectra of the **T4-Mn** (a), **QA-CONs** (b), and the **T4-Mn/QA-CONs** (c).

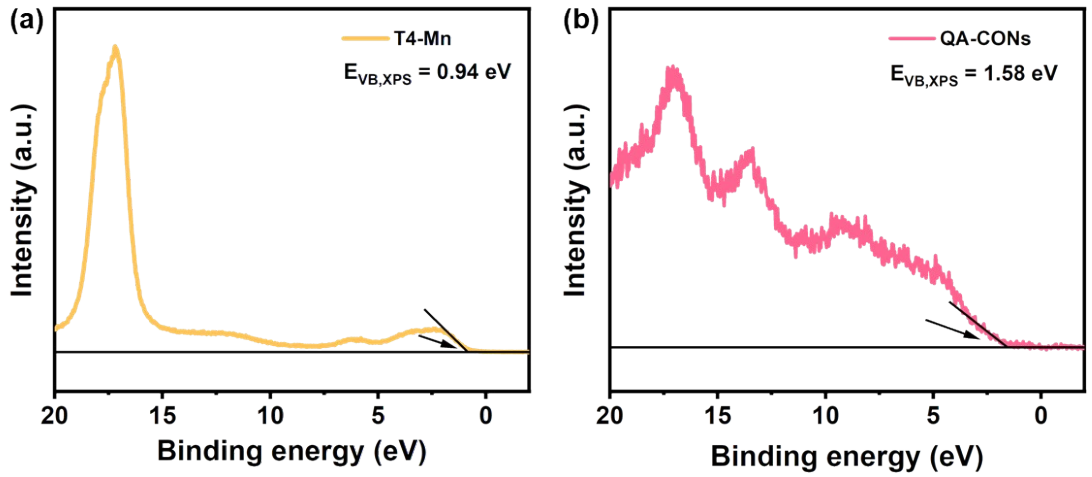

Figure S19. Valence band (VB) XPS spectra of (a) **T4-Mn** and (b) **QA-CONs**.

Note: As depicted in Figure S16, **T4-Mn** exhibits a distinct VB with the edge of maximum energy at about 0.94 eV, while **QA-CONs** display a distinct VB with the edge of maximum energy at around 1.58 eV. The E_{VB} of the corresponding standard hydrogen electrode can be calculated according to the following formula: $E_{VB}(NHE) = \phi + E_{VB,\,XPS} - 4.44$, where ϕ is the work function of the instrument (4.2 eV). Therefore, the calculated E_{VB} of **T4-Mn** and **QA-CONs** are 0.70 V and 1.34 V, respectively.

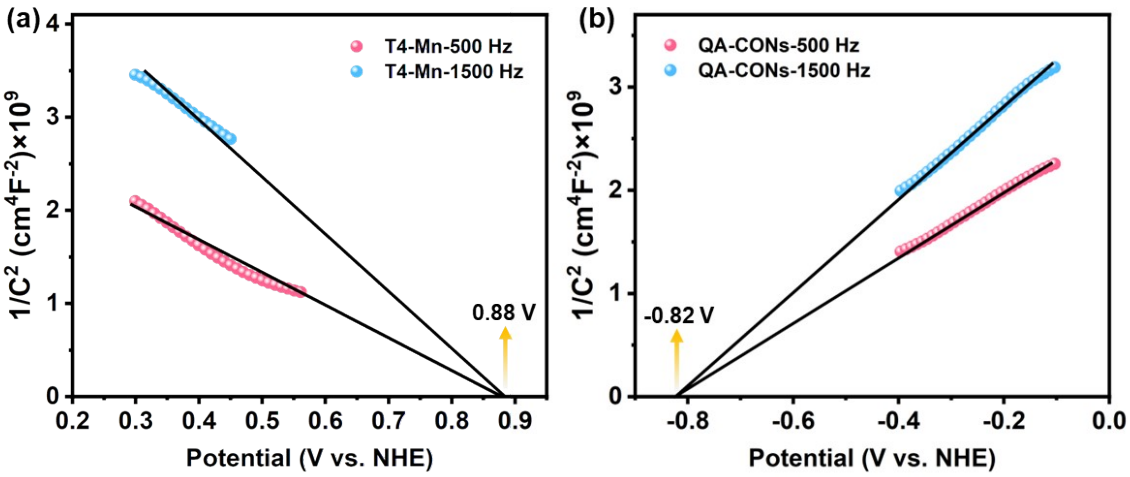

Figure S20. Mott-Schottky plots for **T4-Mn** and **QA-CONs**.

Note: To further investigate the conduction band (CB) and valence band (VB), Mott−Schottky plots were measured for both **T4-Mn** and **QA-CONs**. In general, the E_{VB} for *p*-type semiconductors is very close to the flat-band potential, while the E_{CB} for *n*-type semiconductors closely aligns with the flat-band potential value. Typically, the flat band potential in *n*-type semiconductors is 0.1-0.3 V higher than the CB potential; and this is 0.1-0.3 V lower than the VB potential of *p*-type semiconductors. As displayed in Figure S17 a and b, the $E_{VB,\,\textbf{T4-Mn}}$ and the $E_{CB,\,\textbf{QA-CONs}}$ could be confirmed to

be at 0.88 V (vs. NHE) and -0.82 V (vs. NHE), respectively. Therefore, the $E_{VB,\ \textbf{T4-Mn}}$ and the $E_{CB,\ \textbf{QA-CONs}}$ could be estimated to be 0.98 V and −0.92 V. Based on the formula $E_g = E_{CB} - E_{VB}$, the corresponding E_{CB} of **T4-Mn** and E_{VB} of **QA-CONs** would be approximately -2.10 V and 1.30 V, respectively.

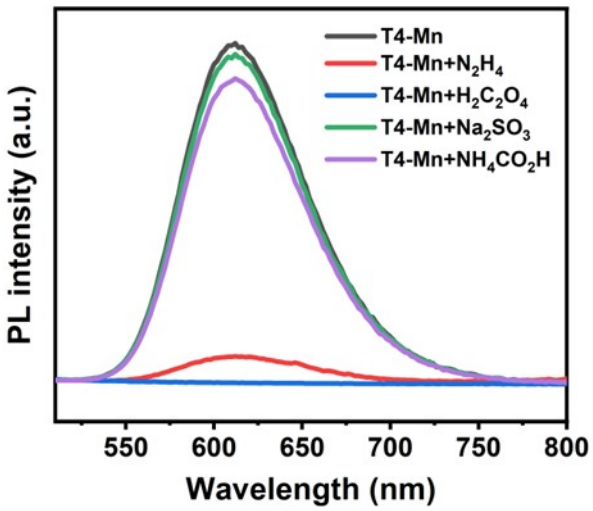

Figure S21. PL spectra (Ex = 365 nm) of **T4-Mn** with or without various sacrificial reagents.

Note: We conducted fluorescence quenching experiments to verify whether the sacrificial agents and **T4-Mn/QA-CONs** exhibit charge transfer behavior. As displayed in Fig. S21, adding hydrazine hydrate to **T4-Mn** results in significant quenching of its emission intensity, confirming charge transfer between them. However, when sodium sulfite and ammonium oxalate are added, no significant change in the PL of **T4-Mn**, suggesting that they may not align well with the energy levels of **T4-Mn**, hindering charge transfer. Notably, due to its moderately strong acidity, oxalic acid leads to the destruction of **T4-Mn** in solution, rendering the PL of **T4-Mn** disappeared completely.

MS spectra of the compounds

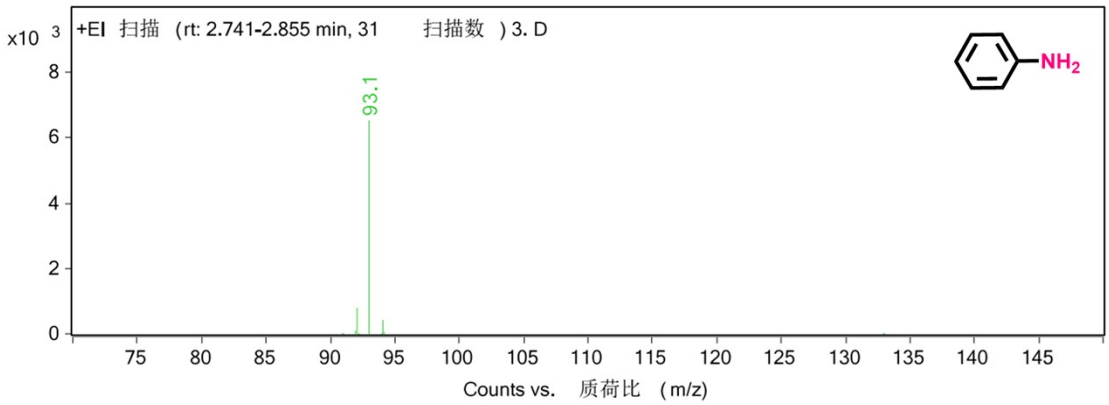

Figure S22. MS of aniline.

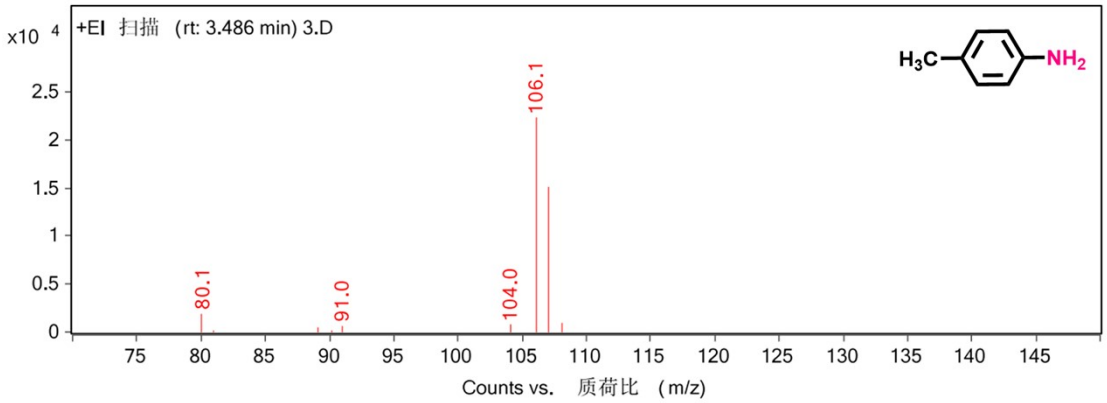

Figure S23. MS of *p*-methylaniline.

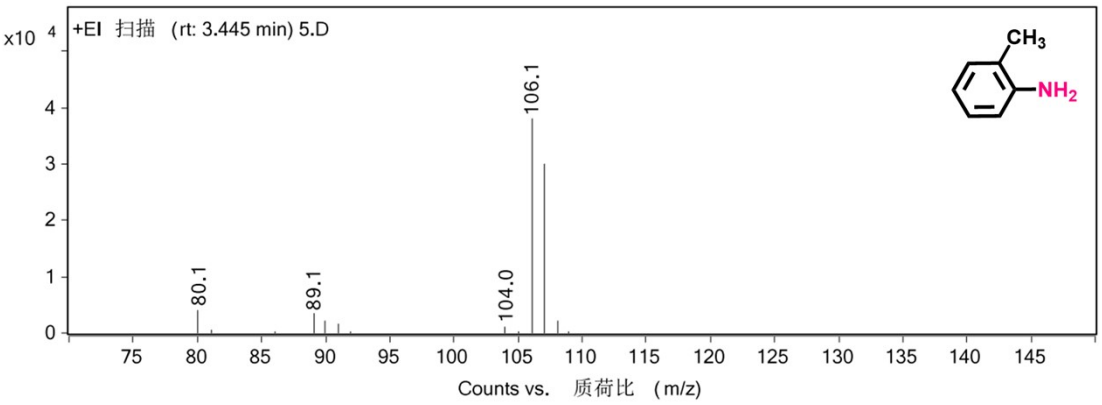

Figure S24. MS of *o*-methylaniline.

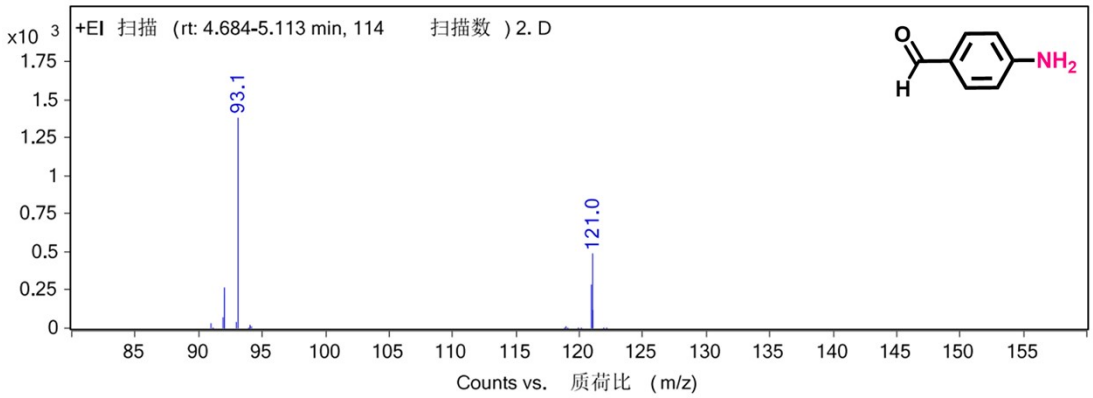

Figure S25. MS of *p*-aminobenzaldehyde.

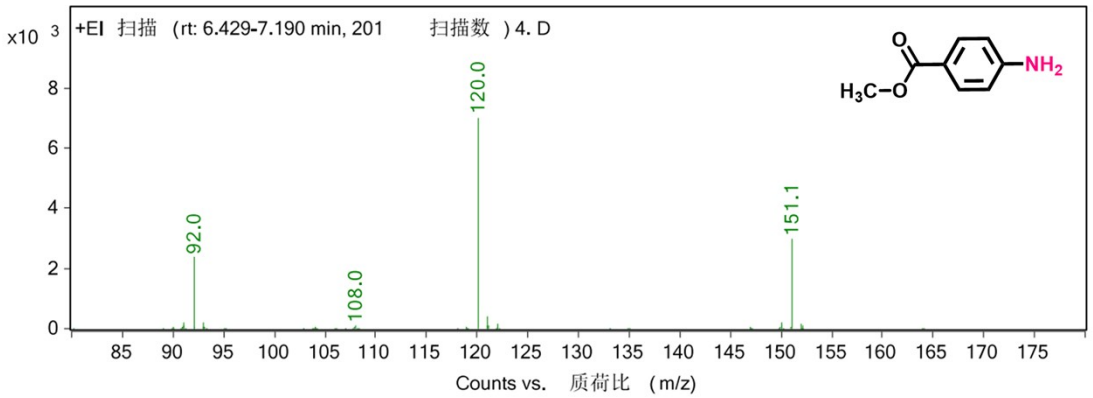

Figure S26. MS of methyl 4-aminobenzoate.

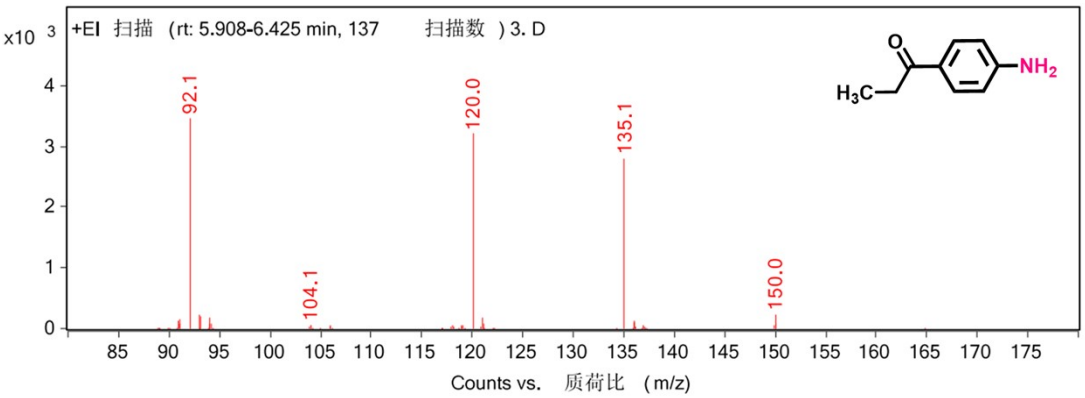

Figure S27. MS of *p*-aminopropiophenone.

Table S1. Comparison of the **T4-Mn/QA-CONs** in terms of TOF for photocatalytic aromatic nitro-reduction reactions[1].

Entry	Irradiation power	Substrate (concentration)	Hydrogen donor/ hole scavengers	Catalyst (amount)	Yield (%)	Reaction time (h)	TOF (h^{-1})	Reference
1	400 W	Nitrobenzene (30 µmol)	methylamine (100 µmol)	TiO_2 (50 mg)	99	4	0.01	[2]Appl. Catal. B Enviorn. 2020
2	300 W	Nitrobenzene (100 µmol)	hydrazine (10 mmol)	P/N co-doped C (10 mg)	100	6	0.02	[3]Appl. Surf. Sci. 2019
3	300 W	Nitrobenzene (125 µmol)	benzotrifluoride (15 mL)	$CdLa_2S_4$ (100 mg)	55.9	10	0.03	[4]Appl. Catal. B Environ. 2018
4	500 mW /cm^2	Nitrobenzene (100 µmol)	KOH (0.1 M)/IPA	$Au_{2.6}Cu_{0.4}@ZrO_2$ (50 mg)	100	6	0.04	[5]ACS Catal. 2016
5	300 W	Nitrobenzene (125 µmol)	benzotrifluoride (15 mL)	0.03% Pt/CdS (100 mg)	70	4	0.04	[6]J. Hazard. Mater. 2018
6	500 W	Antibiotic CAP (2 mg)	H_2O 100 mL	$(CeMoO_4)_2$ /GO (50 mg)	100	0.8	0.09	[7]ACS Appl. Mater. Interfaces 2017
7	300 W	Nitrobenzene (500 µmol)	methanol (50 mL)	$TiO_2/C_3N_4/G$ (100 mg)	97	4	0.10	[8]Appl. Catal. B Environ. 2017

8	300 W	Nitrobenzene (80 µmol)	Pr-OH (4 mL)	TiO_2/C (10 mg)	100	6	0.12	[9]ACS Sustainable Chem. Eng. 2019
9	125 W	Nitrobenzene (40 µmol)	H_2O and MeOH (100 mL)	TiO_2 (50 mg)	100	0.5	0.12	[10]Sci. Rep. 2017
10	20 W	Nitrobenzene (100 µmol)	hydrazine (1 mmol) CH_3CN	$Fe(bpy)_3$/rGO (25 mg)	88	12	0.15	[11]Appl. Surf. Sci. 2016
11	300 W	Nitrobenzene (9.75 µmol)	methanol (10 mL)	Bi_2MoO_6	96.5	1	0.19	[12]Appl. Catal. B Environ. 2019
12	75 W /m^2	Nitrobenzene (1 mmol)	methanol (10 mL)	Ag-rGO/g-C_3N_4 (50 mg)	100	4	0.29	[13]J. Hazard. Mater. 2020
13	0.4 W /cm^2	Nitrobenzene (0.066 mmol)	1 mL H_2O/0.5 mL TEOA 4 mL 1,4-dioxane	TC_5 (15 mg)	99	1.5	0.38	[14]ACS Catal. 2022
14	90 W	Nitrobenzene (150 µmol)	Na_2S/Na_2SO_3 5 mL H_2O	Ni_2P/CdS (2 mg)	100	24	0.45	[15]Chem. Comm. 2015, 51
15	40 mW /cm^2	2,4,6 TNT (3.5 µmol)	CH_3CN/H_2O (0.7/1 mL)	TiO_2/Pt (420 µg)	27	1	0.61	[16]ACS Appl. Mater. Interfaces 2018
16	300 W	Cl-Nitrobenzene (0.5 mmol)	$HCOONH_4$ (3.5 mmol)	AuPt/HTi_2O_4 (20 mg)	99	4	0.92	[17]ACS Catal. 2018

17	400 W	Nitrobenzene (0.2 mmol)	$Na_2S/Na_2SO_3/H_2O$	$Zn_{1-x}Cd_xS$ (5 mg)	99	4	1.10	[18]ACS Sustainable Chem. Eng. 2017
18	450 mW /cm^2	Nitrobenzene (100 µmol)	0.5 mL H_2O/1 bar H_2	Cu_7S_4-Pd (50 mg)	100	0.5	1.55	[19]Nano Lett. 2015
19	300 W	Nitrobenzene (0.5 mmol)	$Na_2S/Na_2SO_3/H_2O$	CuxS-ZnCdS (20 mg)	100	1.8	3.90	[20]Nano Res. 2018
20	300 W	Nitrobenzene (100 µmol)	hydrazine (0.1 mmol) in 1 mL EtOH	Zn-MOF (5 mg)	100	4	13.3	[21]J Mater. Chem. A 2019
21	300 mW /cm^2	Nitroarenes (6 mmol)	H_2 atm. flow	$Pd_3Au_{0.5}$/SiC (25 mg)	80	0.5	7.90	[22]ACS Appl. Mater. 2018
22	34 W 22 mW /cm^2	Nitrobenzene (1 mmol)	Hydrazine, 16 mmol in 1 mL H_2O	$CuFeS_2$ (2 mg)	99.4	4	22.8	[1]Nat Nanotechnol. 2022
23	**6 W**	**Nitrobenzene (100 µmol)**	**Hydrazine, 0.5 mmol in 3 mL H_2O/CH_3CN**	**T4-Mn/QA-CONs (2.3 mg)**	**99**	**10**	**2.68**	**This work**

Table S2. Lifetime (τ_i) and amplitudes (A_i) of the transient absorption decays at 450 nm for **T4-Mn**, **QA-CONs**, and **T4-Mn/QA-CONs** (pump = 320 nm).

λ = 450 nm	**τ_1 (ps)**	**A_1 (%)**	**τ_2 (ps)**	**A_2 (%)**	**τ_3 (ps)**	**A_3 (%)**	**τ_4 (ps)**	**A_4 (%)**
T4-Mn	4.65±0.49	11.01	0.45±0.04	88.25	>138.95±11.04	0.73	——	——
QA-CONs	2.95±0.1	77.44	>32.73±1.95	22.56	——	——	——	——
T4-Mn/QA-CONs	14.80±2.65	23.43	733.4±11.10	3.33	1.32±0.12	68.88	>174.4±27.70	4.36

II. References

1. Cheruvathoor Poulose, A.; Zoppellaro, G.; Konidakis, I.; Serpetzoglou, E.; Stratakis, E.; Tomanec, O.; Beller, M.; Bakandritsos, A.; Zbořil, R., Fast and selective reduction of nitroarenes under visible light with an earth-abundant plasmonic photocatalyst. *Nat. Nanotechnol.* **2022**, *17* (5), 485-492.

2. Fukui, M.; Koshida, W.; Tanaka, A.; Hashimoto, K.; Kominami, H., Photocatalytic hydrogenation of nitrobenzenes to anilines over noble metal-free TiO_2 utilizing methylamine as a hydrogen donor. *Appl. Catal. B Environ.* **2020**, *268*. 118446.

3. Zhang, H.; Zhang, C.; Zhang, Y.; Cui, P.; Zhang, Y.; Wang, L.; Wang, H.; Gao, Y., P/N co-doped carbon derived from cellulose: A metal-free photothermal catalyst for transfer hydrogenation of nitroarenes. *Appl. Surf. Sci.* **2019**, *487*, 616-624.

4. Zhang, S.; Huang, W.; Fu, X.; Zheng, X.; Meng, S.; Ye, X.; Chen, S., Photocatalytic organic transformations: Simultaneous oxidation of aromatic alcohols and reduction of nitroarenes on $CdLa_2S_4$ in one reaction system. *Appl. Catal. B Environ.* **2018**, *233*, 1-10.

5. Xiao, Q.; Sarina, S.; Waclawik, E. R.; Jia, J.; Chang, J.; Riches, J. D.; Wu, H.; Zheng, Z.; Zhu, H., Alloying Gold with Copper Makes for a Highly Selective Visible-Light Photocatalyst for the Reduction of Nitroaromatics to Anilines. *ACS Catal.* **2016**, *6* (3), 1744-1753.

6. Zhang, S.; Huang, W.; Fu, X.; Chen, G.; Meng, S.; Chen, S., Ultra-low content of Pt modified CdS nanorods: Preparation, characterization, and application for photocatalytic selective oxidation of aromatic alcohols and reduction of nitroarenes in one reaction system. *J. Hazard. Mater.* **2018**, *360*, 182-192.

7. Karthik, R.; Vinoth Kumar, J.; Chen, S.-M.; Karuppiah, C.; Cheng, Y.-H.; Muthuraj, V., A Study of Electrocatalytic and Photocatalytic Activity of Cerium Molybdate Nanocubes Decorated Graphene Oxide for the Sensing and Degradation of Antibiotic Drug Chloramphenicol. *ACS Appl. Mater. Interfaces* **2017**, *9* (7), 6547-6559.

8. Zhang, L.; He, X.; Xu, X.; Liu, C.; Duan, Y.; Hou, L.; Zhou, Q.; Ma, C.; Yang, X.; Liu, R.; Yang, F.; Cui, L.; Xu, C.; Li, Y., Highly active TiO_2/g-C_3N_4/G photocatalyst with extended spectral response towards selective reduction of nitrobenzene. *Appl. Catal. B Environ.* **2017**, *203*, 1-8.

9. Xu, S.; Tang, J.; Zhou, Q.; Du, J.; Li, H., Interfacing Anatase with Carbon Layers for Photocatalytic Nitroarene Hydrogenation. *ACS Sustainable Chem. Eng.* **2019**, *7* (19), 16190-16199.

10. Challagulla, S.; Tarafder, K.; Ganesan, R.; Roy, S., Structure sensitive photocatalytic reduction of nitroarenes over TiO_2. *Sci. Rep.* **2017**, *7*. 8783.

11. Kumar, A.; Kumar, P.; Paul, S.; Jain, S. L., Visible light assisted reduction of nitrobenzenes using $Fe(bpy)_3$/rGO nanocomposite as photocatalyst. *Appl. Surf. Sci.* **2016,** *386*, 103-114.

12. Xie, Y.; Shang, X.; Liu, D.; Zhao, H.; Gu, Y.; Zhang, Z.; Wang, X., Non-noble metal thickness-tunable Bi_2MoO_6 nanosheets for highly efficient visible-light-driven nitrobenzene reduction into aniline. *Appl. Catal. B Environ.* **2019**, *259*. 118087.

13. Kumar, A.; Paul, B.; Boukherroub, R.; Jain, S. L., Highly efficient conversion of the nitroarenes to amines at the interface of a ternary hybrid containing silver nanoparticles doped reduced graphene oxide/ graphitic carbon nitride under visible light. *J. Hazard. Mater.* **2020,** *387*. 121700.

14. Xu, F.; Meng, K.; Cao, S.; Jiang, C.; Chen, T.; Xu, J.; Yu, J., Step-by-Step Mechanism Insights into the TiO_2/Ce_2S_3 S-Scheme Photocatalyst for Enhanced Aniline Production with Water as a Proton Source. *ACS Catal.* **2021**, *12* (1), 164-172.

15. Gao, W.-Z.; Xu, Y.; Chen, Y.; Fu, W.-F., Highly efficient and selective photocatalytic reduction of nitroarenes using the Ni_2P/CdS catalyst under visible-light irradiation. *Chem. Comm.* **2015**, *51* (67), 13217-13220.

16. Kong, L.; Mayorga-Martinez, C. C.; Guan, J.; Pumera, M., Fuel-Free Light-Powered TiO_2/Pt Janus Micromotors for Enhanced Nitroaromatic Explosives Degradation. *ACS Appl. Mater. Interfaces* **2018**, *10* (26),

22427-22434.

17. Song, Y.; Wang, H.; Wang, Z.; Guo, B.; Jing, K.; Li, Y.; Wu, L., Selective Photocatalytic Synthesis of Haloanilines from Halonitrobenzenes over Multifunctional AuPt/Monolayer Titanate Nanosheet. *ACS Catal.* **2018**, *8* (10), 9656-9664.

18. Kaur, M.; Nagaraja, C. M., Template-Free Synthesis of $Zn_{1-x}Cd_xS$ Nanocrystals with Tunable Band Structure for Efficient Water Splitting and Reduction of Nitroaromatics in Water. *ACS Sustainable Chem. Eng.* **2017**, *5* (5), 4293-4303.

19. Cui, J.; Li, Y.; Liu, L.; Chen, L.; Xu, J.; Ma, J.; Fang, G.; Zhu, E.; Wu, H.; Zhao, L.; Wang, L.; Huang, Y., Near-Infrared Plasmonic-Enhanced Solar Energy Harvest for Highly Efficient Photocatalytic Reactions. *Nano Lett.* **2015**, *15* (10), 6295-6301.

20. Yu, Z.; Chen, Z.; Chen, Y.; Peng, Q.; Lin, R.; Wang, Y.; Shen, R.; Cao, X.; Zhuang, Z.; Li, Y., Photocatalytic hydrogenation of nitroarenes using $Cu_{1.94}S$-$Zn_{0.23}Cd_{0.77}S$ heteronanorods. *Nano Res.* **2018**, *11* (7), 3730-3738.

21. Chen, P.; Guo, Z.; Liu, X.; Lv, H.; Che, Y.; Bai, R.; Chi, Y.; Xing, H., A visible-light-responsive metal–organic framework for highly efficient and selective photocatalytic oxidation of amines and reduction of nitroaromatics. *J. Mater. Chem. A* **2019**, *7* (47), 27074-27080.

22. Hao, C.-H.; Guo, X.-N.; Sankar, M.; Yang, H.; Ma, B.; Zhang, Y.-F.; Tong, X.-L.; Jin, G.-Q.; Guo, X.-Y., Synergistic Effect of Segregated Pd and Au Nanoparticles on Semiconducting SiC for Efficient Photocatalytic Hydrogenation of Nitroarenes. *ACS Appl. Mater. Interfaces* **2018**, *10* (27), 23029-23036.